Field emission and strain engineering of electronic properties in boron nitride nanotubes

2012 Nanotechnology 23 105702

(http://iopscience.iop.org/0957-4484/23/10/105702)

Nanotechnology **23** (2012) 105702 (6pp) doi:10.1088/0957-4484/23/10/105702

Field emission and strain engineering of electronic properties in boron nitride nanotubes

Hessam M Ghassemi[1], Chee Hui Lee[2], Yoke Khin Yap[2] and Reza S Yassar[1]

[1] Department of Mechanical Engineering-Engineering Mechanics, Michigan Technological University, 1400 Townsend Dr, Houghton, MI 49931, USA
[2] Department of Physics, Michigan Technological University, 1400 Townsend Dr, Houghton, MI 49931, USA

E-mail: ykyap@mtu.edu and reza@mtu.edu

Received 16 December 2011, in final form 28 January 2012
Published 21 February 2012
Online at stacks.iop.org/Nano/23/105702

Abstract
The electrical properties of boron nitride (BN) nanostructures, particularly BN nanotubes (NTs), have been studied less in comparison to the counterpart carbon nanotubes. The present work investigates the field emission (FE) behavior of BNNTs under multiple cycles of FE experiments and demonstrates a strain-engineering pathway to tune the electronic properties of BNNTs. The electrical probing of individual BNNTs were conducted inside a transmission electron microscope (TEM) using an *in situ* electrical holder capable of applying a bias voltage of up to 110 V. Our results indicate that in the first cycle a single BNNT can exhibit the current density of $\sim$1 mA cm^{-2} at 110 V and the turn-on voltage of 325 V μm^{-1}. However, field emission properties reduced considerably in subsequent cycles. Real-time imaging revealed the structural degradation of individual BNNTs during FE experiments. The electromechanical measurements show that the conductivity of BNNTs can be tuned by means of mechanical straining. The resistance of individual BNNTs reduced from 2000 to 769 MΩ and the carrier concentration increased from 0.35×10^{17} to 1.1×10^{17} cm^{-3} by straining the samples up to 2.5%.

(Some figures may appear in colour only in the online journal)

1. Introduction

Boron nitride nanotubes (BNNTs) are not only structurally similar to carbon nanotubes (CNTs) [1], but their mechanical properties are also calculated and measured to be comparable to those of the CNTs [2, 3]. However, BNNTs show insulating behavior due to a wide bandgap of 5.4 eV [4]. Theoretical simulations predict that the electronic properties in BNNTs can be tuned by means of mechanical deformation or chemical alteration. Kim *et al* [5] concluded that the bandgap of BNNTs was reduced as the cross section of the nanotubes became oval under bending deformation. Their density functional calculations showed that the redistribution of charges is more significant in the conduction band compared to that of the valence band. Golberg *et al* [6] altered the BN structure by adding carbon and facilitating the formation of B–C–N layers. Their electrical and field emission (FE) results showed significant improvement in the measured conductivity.

The superior antioxidation ability of BNNTs in comparison to CNTs justifies their candidacy for FE applications [7]. Thermogravimetry analysis shows that BNNTs are stable up to 950 °C, while CNTs decompose at 500 °C [8]. *In situ* transmission electron microscopy (TEM) observations also showed electrical failure of CNTs takes place at a voltage range of $\pm$7 V whereas BNNTs could withstand up to $\pm$140 V with no electrical breakdown or physical failure [9]. *In situ* FE experiments conducted by Cumings *et al* [10] on individual BNNTs showed stable current at high bias voltages. However, they did not study the stability of emission current under multi-cycle measurements. Since long-term

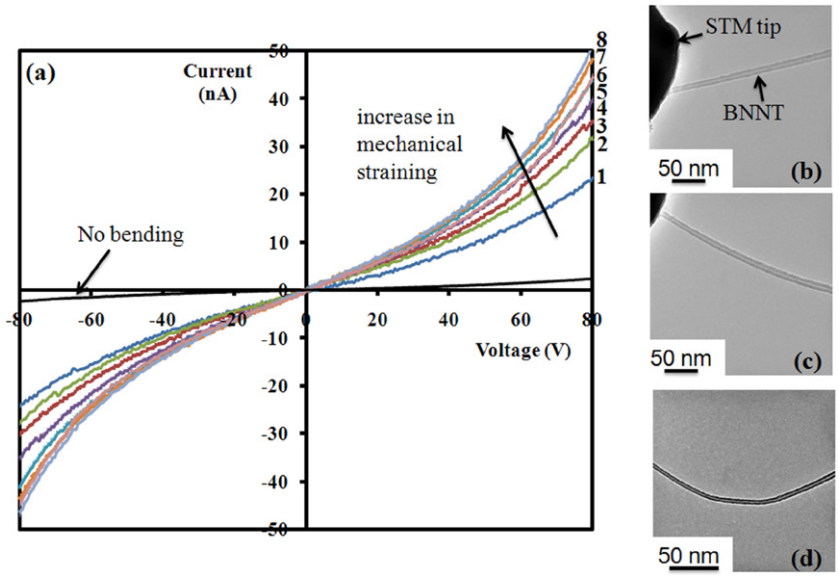

Figure 1. (a) The corresponding *I–V* curves of a BNNT under mechanical straining. The colored curves indicate the *I–V* data during progressive strain loading and the black curve (marked with a short arrow) shows the insulating behavior under no bending. (b) The TEM image of a BNNT in contact with STM tip (no loading) corresponds to the black curve in (a). (c), (d) The TEM images of BNNTs under the continuous increase of mechanical straining, respectively. The bending curvatures of the BNNT increase due to higher mechanical straining. *I–V* curves 1 and 8 represent cases with the lowest to highest amount of bending.

emission stability is one of the major factors that prevents practical applications of nanotubes [11]. Thus it is important to further understand the FE cycling performance of BNNTs for potential applications in flat panel displays.

In this work, we first tuned the electrical properties of BNNTs under mechanical deformation. The mechanical deformation was performed on individual BNNTs inside the chamber of a TEM using an *in situ* scanning tunneling microscopy (STM) holder. Electrical and semiconducting properties of BNNTs were measured under different strain levels. Then, we evaluated the FE stability of individual BNNTs. TEM images were captured after each cycle of FE experiments to study the possible relation between the emission stability and the structural integrity of BNNTs.

2. Materials and methods

Our BNNTs were directly deposited on Si substrates by thermal chemical vapor deposition at 1100–1200 °C in a conventional tube furnace [12]. These BNNTs have a bandgap of 6 eV [12], which is higher than those reported in previous works (∼5.4 eV) [13–15]. The conductivity probing experiments were performed in a STM holder under *in situ* monitoring in a JEOL JEM-4000FX, operated at 200 kV. Individual BNNTs were then attached on an Au wire by either light mechanical scratching on the as-grown samples or using silver paste. This Au wire was then fixed on the tip of a piezo-driven holder that allowed nanometer motion of the sample towards the STM tip. The sample position was adjustable with a precision of 1 nm in the *X*, *Y* and *Z* directions. Here, the sample was grounded and positive bias voltages were applied to the STM tip. Then the *I–V* curves were measured using the Nanofactory^{TM} instrument (up to ±80 V) power generator. To reduce the effect of electron beam irradiation on the nanotubes during *I–V* measurements, the electron beam current of the TEM was reduced to half of that we use for normal imaging. For the FE experiments, BNNTs were retraced away from the STM tip and then were biased with negative range voltage to emit electrons. The applied range of voltage started from zero up to 110 V within 20–60 s. To enhance the accuracy of current measurements, a flat part of the STM tip was used to collect the emission current. Because of insulating behavior of BNNTs and voltage limitation of our set-up, a short distance between the tip of BNNTs and the STM tip was used to form a sufficient electric field for capturing the emission current from BNNTs.

3. Results and discussion

3.1. Strain engineering of electrical conductivity in BNNTs

Figure 1(a) represents *I–V* behaviors of individual BNNTs under continued increase of mechanical straining. The black curve near the *X* axis shows a current flow of a few nanoamperes at 80 V applied voltage, indicating the insulating behavior of pure BNNTs with no bending deformation (corresponding to figure 1(b)). Our calculations revealed that the resistance of pure non-deformed BNNTs is around 10 GΩ, which is in good agreement with the reported values [16].

Next, the nanotube was subjected to a series of mechanical straining while *I–V* data were simultaneously collected. Figures 1(c) and (d) represent two different bending curvatures of the BNNT (shown in figure 1(a)) under different applied forces. The colored curves in figure 1(a), labeled as 1–8, represent the *I–V* curves at different bending curvatures. The applied stress changes the conductivity of BNNTs; hence,

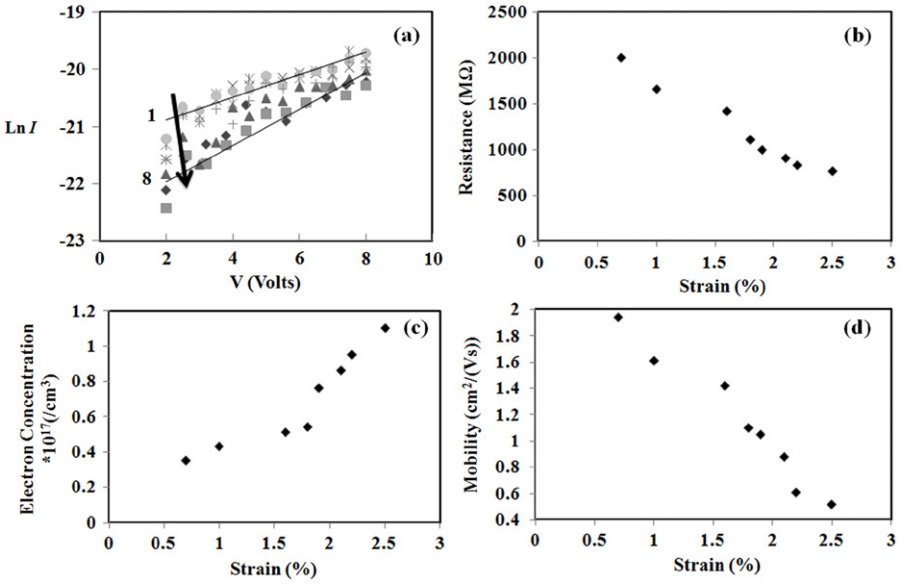

Figure 2. (a) Characteristic ln *I*–*V* data corresponding to the *I*–*V* curves shown in figure 1(a). Arrow from 1–8 indicates the increase in the bending deformation. (b)–(d) represent the parameters of resistance, electron concentration and mobility of the bent BNNT as a function of mechanical straining.

higher current flows were detected at higher strain levels (corresponding to 1–8 in figure 1(a)).

One can notice from figure 1(a) that *I*–*V* curves are not symmetric, for instance, the red curve, labeled as 3, at 80 V leads to a current of 35 nA whereas the current detected at −80 V was −30 nA. These asymmetric *I*–*V* behaviors are due to different contact barriers at both ends of the BNNT. As mentioned in the experimental procedure, one end of the nanotube is in contact with the tungsten STM tip and the other end is in contact with the gold wire. This can form a metal–semiconductor–metal (M–S–M) circuit with different work functions and therefore different Schottky barriers [17].

Following the theory of a M–S–M circuit [18], one can calculate the semiconducting parameters of BNNTs by

$$\ln I = \ln S + V\left(\left(\frac{q}{K_{\mathrm{B}}T}\right) - \frac{1}{E_0}\right) + \ln J_{\mathrm{s}} \qquad (1)$$

where S is the contact area associated with a bias and J_{s} is a slowly varying function of the applied bias. The ln I versus V plot gives an approximately straight line with a slope of $\frac{q}{K_{\mathrm{B}}T} - \frac{1}{E_0}$ and an intercept of ln S, as shown in figure 2(a). In this case, $E_0 = E_{00}\coth[E_{00}/(k_{\mathrm{B}}T)]$, where $E_{00} = (\hbar q/2)\,(n/(m^*\varepsilon))^{1/2}$. Here, $\hbar$ is $1/2\pi$ of the Planck constant, q is the elemental charge, k_{B} is the Boltzmann constant, m^* is an effective electron mass of BNNT, n is carrier concentration and ε is the dielectric constant. The electron mobility, μ, is then calculated by using the relationship $\mu = 1/(nq\rho)$, where ρ is the resistivity of the strained BNNT estimated from the *I*–*V* curves. The calculated parameters of a BNNT under different bending deformations are plotted as shown in figures 2(b)–(d).

As plotted in figure 2(b), the resistance of the BNNT ($\mathrm{d}V/\mathrm{d}I$) can be tuned in a wide range of 2000–769 MΩ under minimum and maximum bending deformations labeled as curves 1 and 8 in figure 1(a), respectively. Our calculation indicates that the electron concentration increases by a factor of 3 (figure 2(c)). However, the carrier's mobility is decreased (figure 2(d)). The reduction in carrier mobility can be related to the scattering between electron and phonon under the applied electric field [19], or due to the presence of impurities similar to the reported results for graphene [20]. As the nanotube bends, the radius of the curvature in the nanotube's cross section also changes. The theoretical calculations show that the conduction electrons are more sensitive to the induced curvature while the valence electrons remain relatively unaffected [5]. As a result, the charge distribution density across the nanotube diameter changes which decreases the energy difference between the bandgaps. Similarly, it is reported that, in the case of ZnO [21], Bi_2S_3 [22] and BNNT [23], the carrier concentration increases due to bandgap reduction upon the applied stress.

Unfortunately, it will be impossible to compare the exact values of the electronic parameters obtained in this work with the ones reported in [16] for deformed BNNTs. This is because in [16] the change in *I*–*V* characteristics in terms of exact strain values was not quantified. For instance, the value of strain corresponding to the reported carrier concentration of 1.1×10^{17} cm^{-3} for deformed BNNTs in [16] was not given. This point in fact is the strength of the work presented here because for the first time it provides a quantified correlation between the values of strain and the electronic properties of BNNTs.

3.2. Field emission properties

figure 3(a) represents the typical field emission characteristic of an individual BNNT (shown in the inset) under an applied bias voltage. The emission of electrons starts at a particular voltage (∼65 V), also known as the turn-on voltage, where the

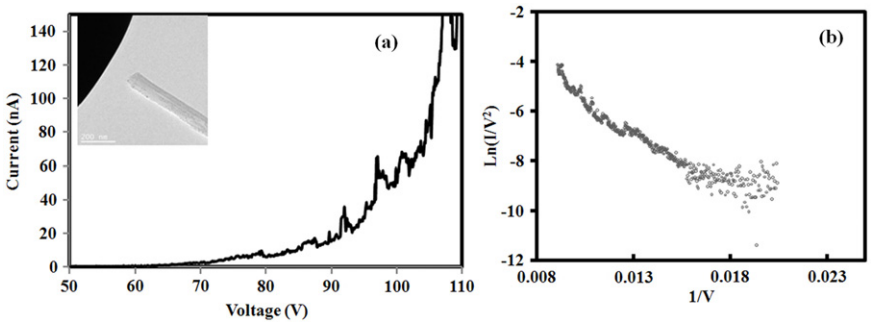

Figure 3. (a) The I–V curve represents the FE behavior of an individual BNNT shown in the inset (first FE cycle). The scale bar is 200 nm. (b) The corresponding Fowler–Nordheim plot representing the field emission behavior shown in (a).

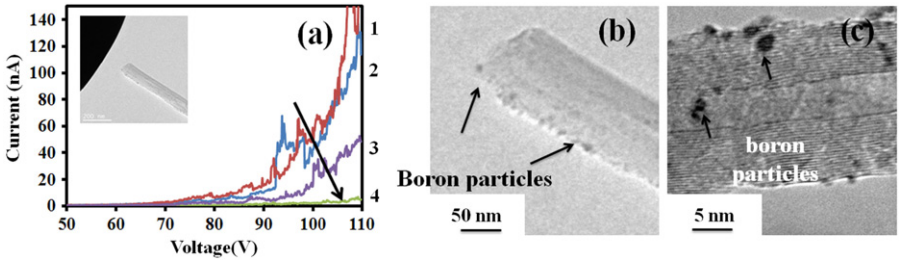

Figure 4. (a) Field emission behaviors of the BNNT at four consecutive measurements. (b), (c) Arrows indicate the formation of black particles as a result of decomposition on the outer surface of the BNNT.

measured current exceeds the background current of 0.5 nA and exponentially increases to 140 nA at 110 V. The turn-on voltage is calculated to be ∼325 V μm^{-1} and the current density of an individual BNNT is measured as ∼1 mA cm^{-2} at a voltage of 110 V.

The FE behavior of this nanotube can be modeled following the well-known Fowler–Nordheim (FN) equation [24], as shown in figure 3(b).

The linear plot of $\ln(I/V^2)$ versus $1/V$ confirms the FN field emission characteristics of the BNNT. One can notice that the BNNT exhibits only one slope which is in good comparison with other reported field emission behaviors of BNNTs [10]. In contrast, the CNTs' FN plot shows two distinct slopes representing current saturation during field emission experiments at high field [25, 26]. Based on the field emission current, one can also calculate other characteristics of the nanotube, such as field enhancement factor, work function and the radius of the apex, as follow [24]:

$$I = KF^2/\phi \exp(-B\phi^{\frac{3}{2}}/F) \tag{2}$$

where $B = 6.8 \times 10^9$ V $eV^{-3/2}$ m^{-1}, K is a constant and ϕ is the sample work function. The local electric field, F, is related to the applied voltage V and can be defined as $F = \beta V/d$, where β, the field enhancement factor, quantifies the ability of amplifying the average field V/d. If S is the slope of the FN plot (figure 3(b)) one can calculate the field enhancement factor using the equation below:

$$S = -B\phi^{\frac{3}{2}}d/\beta. \tag{3}$$

Assuming the work function of pristine BNNT is 6 eV [5], then according to equation (3), $\beta = 98$. The calculated field enhancement factor is significantly higher than the value assumed by Cumings *et al* [10]. They considered $\beta = 10$ and then back-calculated the work function to be ∼11–13 eV. This is extremely high for BNNTs as work functions of 5.5–6 eV have been reported in the literature [12]. Chen *et al* [27] investigated the enhancement in conductivity and the FE behavior of BNNTs coated with Au nanoparticles. In their FE measurement, they assumed that, due to the high quantity and high uniformity of their morphology, the slope of the Fowler–Nordheim plot is only proportional to the work function. Therefore, assuming a work function of 6 eV, they back-calculated the field enhancement factor. Using a fixed enhancement factor for all different samples, they calculated changes in the work function of BNNTs as a result of the Au coating layer.

We then repeated the FE experiment to investigate the structural and emission stability of the BNNT upon four cycles of emission, as illustrated in figure 4(a). Curves 1–4 represent the first, second, third and fourth FE cycles, respectively. As can be seen, in the second cycle, the turn-on voltage is increased to ∼80 V and the emission current dropped slightly to ∼120 nA. FE cycles 3 and 4 represent further degradation of the emission current as well as higher turn-on voltages, respectively. In the fourth cycle the amount of emission current drops almost 90% in comparison to the first cycle.

A previous study showed that the field enhancement factor strongly depended on the geometry of the apex of the emitter [28]. However, our comparison of the tip radius between the pristine and the FE cycled nanotubes did not show any obvious change. Figure 4(b) also shows that the geometry of the BNNT at the tip, compared to the inset in figure 4(a), is

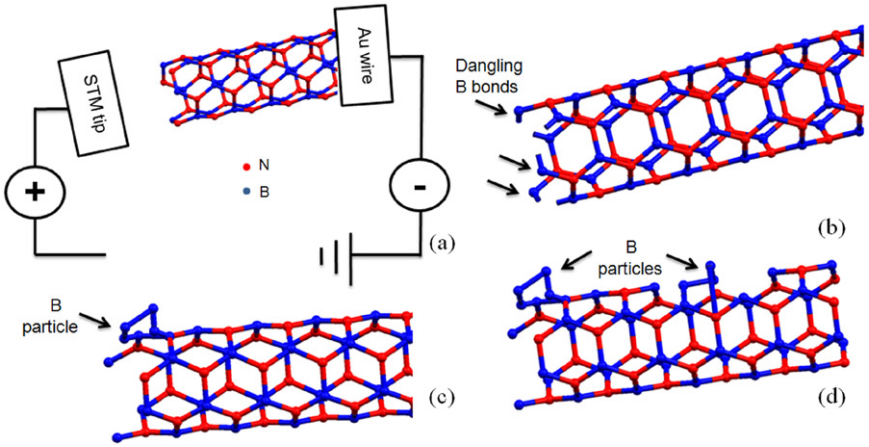

Figure 5. (a) The schematic represents the FE set-up where there is a gap between the tip of the sample and STM tip. As shown, the sample is biased with negative voltage with respect to the STM tip. (b) Arrows indicate the formation of dangling B bonds. The nitrogen atoms leave the structure when the sample reaches the decomposition temperature. (c) and (d) illustrate the formation of boron particles as the number of B atoms with dangling bonds is increased.

not changed significantly. The TEM analysis of the FE cycled nanotube revealed the likelihood of structural decomposition that can explain the reduction in the field enhancement factor. As shown in figures 4(b) and (c), the HRTEM images indicate the presence of dark particles on the outer surface of the FE cycled nanotube. The formation of these particles is due to defects generated by Joule heating, to be discussed hereafter. These defects will cause electron scattering and degrade the emission current.

Figure 5 represents a schematic of the proposed mechanism of the formation of dark particles on the outer surface of the BNNT. As shown in figure 5(a), the sample is biased with negative voltage. As the FE experiments were conducted, due to the high emission current density, the temperature of the sample is increased and reached the decomposition temperature at which the B–N bonds start to break [29]. The volatile nitrogen atoms leave the structure and are released into the vacuum while the B atoms remain (figure 5(b)). As the number of boron atoms with the dangling bond increases, they tend to form particles, as shown in figures 5(c) and (d). Therefore, as the nanotube decomposed, nitrogen which contributes five electrons compared to boron with three electrons leave the structure and the emission current of the nanotube degraded significantly. We should note that several other FE experiments were carried out at the same voltage range of 140 V but at different distances from the STM tip. As the distance between the tip of the nanotube and the STM tip were increased the amount of current also dropped. However, the degradation trend of emission current in FE cycles was also observed, indicating that the observed behavior is independent of the distance between the nanotube and the STM tip.

To rule out the effect of beam damage on the sample, we reduced the accelerating voltage from 300 to 200 kV, and also expanded the beam during the experiments. Moreover, if the decomposition was due to the e-beam radiation, then such a decomposition phenomenon should also be observed during the normal TEM imaging of BNNTs. But, in fact, the formation of particles was only observed when the bias voltage was applied and induced the flow of high density current. In addition, the e-beam radiation should not raise the temperature of the nanotube significantly. Based on the model reported by Jencic *et al* [30], one can calculate that the temperature increase due to the beam exposure at 200 kV and with low electron flux dose is only a few degrees. It should also be mentioned that the formation of dark contrast particles is not due to carbon deposition because the BNNTs that were imaged for a long time without any FE cycles did not show any indication of the particle formation. Therefore, the formation of such particles cannot be due to beam radiation or carbon deposition but rather the FE cycling. Moreover, to minimize any contamination during TEM imaging, the anti-contamination device (ACD) heaters are normally filled with liquid nitrogen prior to the operations.

These results are important in order to understand the mechanism and the performance of the emitters before commercializing them. As mentioned earlier, it is reported that the structure of BNNTs is stable at high temperatures. However, our results show that the repeated cycling under a high electric field can lead to degradation in emission properties. Therefore, it is crucial to employ these findings in the future design and fabrication of BNNT-based nanodevices such as transistors and electromechanical devices [31]. The effect of strain on the electrical characteristics of BNNTs should also be taken into account. For instance, BNNTs can be used as sensors where their conductivity is changed as a result of applied force or strain.

4. Conclusion

We studied the electrical and field emission of individual BNNTs using *in situ* TEM techniques at bias voltages of up to 110 V. Our results showed that individual BNNTs exhibit the current density of $\sim$1 mA cm^{-2} at 110 V and turn-on voltage was 325 V μm^{-1}. However, structural degradation was only observed after four cycles of emitting and the emission current

dropped significantly. Measurements on the semiconducting parameters of individual BNNTs revealed that the bandgap can be tuned by means of mechanical deformation. Based on the amount of strain, the resistance of individual BNNTs was engineered in the range of 2000–769 MΩ and electron concentration was calculated to be 0.35–1.1 $\times$ 10^{17} cm^{-3} in that range of strain with a slight decrease in the mobility of the carriers.

References

[1] Golberg D, Bando Y, Tang C C and Zhi C Y 2007 Boron nitride nanotubes *Adv. Mater.* **19** 2413–32

[2] Ghassemi H M and Yassar R S 2010 On the mechanical behavior of boron nitride nanotubes *Appl. Mech. Rev.* **63** 020804

[3] Zhi C, Bando Y, Tang C and Golberg D 2010 Boron nitride nanotubes *Mater. Sci. Eng.* R **70** 92–111

[4] Blase X, Rubio A, Louie S G and Cohen M L 1994 Stability and band gap constancy of boron nitride nanotubes *Europhys. Lett.* **28** 335

[5] Kim Y-H, Chang K J and Louie S G 2001 Electronic structure of radially deformed BN and BC3 nanotubes *Phys. Rev.* B **63** 205408

[6] Golberg D, Dorozhkin P S, Bando Y, Dong Z C, Tang C C, Uemura Y, Grobert N, Reyes-Reyes M, Terrones H and Terrones M 2003 Structure, transport and field-emission properties of compound nanotubes: CN_x versus BNC_x ($x < 0.1$) *Appl. Phys.* A **76** 499–507

[7] Bonard J-M, Croci M, Klinke C, Kurt R, Noury O and Weiss N 2002 Carbon nanotube films as electron field emitters *Carbon* **40** 1715–28

[8] Golberg D, Bando Y, Kurashima K and Sato T 2001 Synthesis and characterization of ropes made of BN multiwalled nanotubes *Scr. Mater.* **44** 1561–5

[9] Golberg D, Costa P, Mitome M and Bando Y 2008 Nanotubes in a gradient electric field as revealed by STM TEM technique *Nano Res.* **1** 166–75

[10] Cumings J and Zettl A 2004 Field emission and current–voltage properties of boron nitride nanotubes *Solid State Commun.* **129** 661–4

[11] Pandey A, Prasad A, Moscatello J P and Yap Y K 2010 Stable electron field emission from PMMA-CNT matrices *ACS Nano* **4** 6760–6

[12] Lee C H, Wang J, Kayatsha V K, Huang J Y and Yap Y K 2008 Effective growth of boron nitride nanotubes by thermal chemical vapor deposition *Nanotechnology* **19** 455605

[13] Wang J, Kayastha V K, Yap Y K, Fan Z, Lu J G, Pan Z, Ivanov I N, Puretzky A A and Geohegan D B 2005 Low temperature growth of boron nitride nanotubes on substrates *Nano Lett.* **5** 2528–32

[14] Jaffrennou P, Barjon J, Lauret J S, Maguer A, Golberg D, Attal-Trétout B, Ducastelle F and Loiseau A 2007 Optical properties of multiwall boron nitride nanotubes *Phys. Status Solidi* b **244** 4147–51

[15] Zhi C, Bando Y, Tan C and Golberg D 2005 Effective precursor for high yield synthesis of pure BN nanotubes *Solid State Commun.* **135** 67–70

[16] Bai X, Golberg D, Bando Y, Zhi C, Tang C, Mitome M and Kurashima K 2007 Deformation-driven electrical transport of individual boron nitride nanotubes *Nano Lett.* **7** 632–7

[17] Schottky W 1938 Halbleitertheorie der Sperrschicht *Naturwissenschaften* **26** 843

[18] Padovani F A and Stratton R 1966 Field and thermionic-field emission in Schottky barriers *Solid-State Electron.* **9** 695–707

[19] Dürkop T, Getty S A, Cobas E and Fuhrer M S 2003 Extraordinary mobility in semiconducting carbon nanotubes *Nano Lett.* **4** 35–9

[20] Bolotin K I, Sikes K J, Jiang Z, Klima M, Fudenberg G, Hone J, Kim P and Stormer H L 2008 Ultrahigh electron mobility in suspended graphene *Solid State Commun.* **146** 351–5

[21] Asthana A, Momeni K, Prasad A, Yap Y K and Yassar R S 2009 *In situ* probing of electromechanical properties of an individual ZnO nanobelt *Appl. Phys. Lett.* **95** 172106

[22] Zhang Z, Yao K, Liu Y, Jin C, Liang X, Chen Q and Peng L M 2007 Quantitative analysis of current–voltage characteristics of semiconducting nanowires: decoupling of contact effects *Adv. Funct. Mater.* **17** 2478–89

[23] Golberg D, Bai X D, Mitome M, Tang C C, Zhi C Y and Bando Y 2007 Structural peculiarities of *in situ* deformation of a multi-walled BN nanotube inside a high-resolution analytical transmission electron microscope *Acta Mater.* **55** 1293–8

[24] Fowler R H and Nordheim L 1928 Electron emission in intense electric fields *Proc. R. Soc. Lond.* A **119** 173–81

[25] Bonard J M, Salvetat J P, Stöckli T, Forró L and Châtelain A 1999 Field emission from carbon nanotubes: perspectives for applications and clues to the emission mechanism *Appl. Phys.* A **69** 245–54

[26] Collins P G and Zettl A 1997 Unique characteristics of cold cathode carbon-nanotube-matrix field emitters *Phys. Rev.* B **55** 9391–9

[27] Chen H, Zhang H, Fu L, Chen Y, Williams J S, Yu C and Yu D 2008 Nano Au-decorated boron nitride nanotubes: conductance modification and field-emission enhancement *Appl. Phys. Lett.* **92** 243105

[28] Ducastelle F, Blase X, Bonard J M, Charlier J C and Petit P 2006 Electronic structure *Understanding Carbon Nanotubes* (*Springer Lecture Notes in Physics* vol 677) ed A Loiseau, P Launois, P Petit, S Roche and J-P Salvetat (Berlin: Springer) pp 199–276

[29] Ghassemi H, Lee C, Yap Y and Yassar R 2010 *In situ* TEM monitoring of thermal decomposition in individual boron nitride nanotubes *J. Miner. Met. Mater. Soc.* **62** 69–73

[30] Jencic I, Bench M W, Robertson I M and Kirk M A 1995 Electron-beam-induced crystallization of isolated amorphous regions in Si, Ge, GaP, and GaAs *J. Appl. Phys.* **78** 974–82

[31] Golberg D, Bando Y, Huang Y, Terao T, Mitome M, Tang C and Zhi C 2010 Boron nitride nanotubes and nanosheets *ACS Nano* **4** 2979–93